Influence of Abrasion Treatments on Performance of Adhesively Bonded Glass/Vinyl Ester Single Lap Joints

Abdurohman, Kosim
Research Centre for Aeronautics Technology, National Research and Innovation Agency - BRIN

Rezky Agung Pratomo
Research Centre for Aeronautics Technology, National Research and Innovation Agency - BRIN

Hidayat, Ryan
Research Centre for Aeronautics Technology, National Research and Innovation Agency - BRIN

Redha Akbar Ramadhan
Research Centre for Aeronautics Technology, National Research and Innovation Agency - BRIN

他

https://doi.org/10.5109/7183361

出版情報：Evergreen. 11 (2), pp.806-820, 2024-06. 九州大学グリーンテクノロジー研究教育センター
バージョン：

Influence of Abrasion Treatments on Performance of Adhesively Bonded Glass/Vinyl Ester Single Lap Joints

Kosim Abdurohman[1,2*], Rezky Agung Pratomo[1,2], Ryan Hidayat[1,2], Redha Akbar Ramadhan[1,2], Taufiq Satrio Nurtiasto[1,2], Riki Ardiansyah[1,2], Mikhael Gilang P.P.P. [1,2], Fajar Ari Wandono[1,2]

[1]Research Centre for Aeronautics Technology, National Research and Innovation Agency - BRIN, Indonesia
[2]Research Group of Aerostructure, National Research and Innovation Agency - BRIN, Indonesia

*Author to whom correspondence should be addressed:
E-mail: kosi001@brin.go.id

(Received October 6, 2023; Revised March 7, 2024; Accepted April 21, 2024).

Abstract: Composites are frequently used in lightweight constructions, such as aeroplanes and automobiles. In its application, joints such as adhesively bonded joints exist in composite structures. The effect of sanding treatments on Glass Fibre Reinforced Polymer (GFRP) composite with various grit sizes on the surface arithmetic average of the roughness profile, surface topography, liquid contact angle, and single lap joints shear strength was investigated in this research to improve the bonding characteristics of composites for future utilisation in structural adhesion applications. Scanning electron microscopy analysis was conducted to assess the fracture surface of the specimen post-testing. This work's primary objective was to compare the effectiveness of treated surfaces to untreated surfaces when it came to improving the adhesion quality of composites. A surface roughness tester was utilized to estimate the surface arithmetic average of the roughness profile. An atomic force microscope was utilised to analyse the morphology of the composite surface. The contact angle machine was applied to evaluate the liquid contact angle of the composite surfaces. The single lap shear joint test was used to assess the shear strength of composite bonded joints. The results of tests showed that the composite bonded joints' shear strength was maximum in specimens treated with a grit 800 sandpaper belt. These specimens had the lowest liquid contact angle and a consistent peak surface topography. Fibres were exposed at the composite's surface due to the sanding process. The bonded joints' shear strength and the composite's surface condition were impacted by the different grit sizes employed throughout the sanding process. Compared to untreated composite, sanding treatments utilising different grit sizes of sandpaper belts improved the composite's adhesive qualities. Scanning electron microscopy analysis showed that bonding occurs between adhesive and fibre in sanded specimens, whereas not in untreated specimens.

Keywords: composite; adhesive; sanding; surface morphology; contact angle; single lap joints

1. Introduction

Given the manufacturing sector's recent rapid growth, the development of materials concerning fatigue qualities and sustainability is necessary. One material that has evolved that satisfies these property requirements and has potential in a variety of applications is composites[1)]. Due to its high specific strength, failure strain, and specific stiffness, composites are frequently used in lightweight constructions, such as aeroplanes and automobiles[2–5)]. In recent years, fibre-reinforced polymer materials have replaced stainless steel and similar resources in the aviation and aerospace sectors due to superior corrosion resistance, low thermal expansion capacity, and excellent damping[6,7)]. Its use has also increased in the automotive, marine, military, wind turbine, sports, and civil engineering industries[2,6)]. The vast range of sectors in which composites are used has led to a growing interest in developing dependable joining techniques for composite components[2)]. However, composites have drawbacks that restrict their use, such as weak fracture toughness and significant moisture absorption[8)].

Mechanical joints and adhesive joints are the two types of joints. In contrast to adhesive joints, which employ an adhesive interlayer between the adherends, a mechanical joint is often made by securing the adherends using rivets or bolts. An adhesive joint has better fatigue resistance, can transmit load over a broader surface than a mechanical joint, contributes minimal weight to the structure, requires no holes, and does not necessitate perforations. Hence, adhesive joints are extensively utilised for the bonding of

composite materials. However, an adhesive joint is difficult to disassemble for inspection and repair, needs precise preparation of the adherend surfaces, and is impacted by service conditions[9].

However, adhesive or bonded joints exhibit greater intricacy compared to mechanical joints. Various service environments, the temperature and humidity of the place where the attachment joints are used, shall be considered when dealing with adhesives. Furthermore, within the manufacturing process, the finishing of composite permits us to accomplish specified surface finish, geometric structure, and precision through the various treatments to achieve an acceptable level of bond[10]. More complex and careful surface treatment is particularly needed concerning the adhesion joining of long areas or thin composites[11].

There are currently several surface treatment methods used for composite joints, such as plasma processing[12,13], flame treatments, ultraviolet disinfection[14,15], coupling agents, CO_2 laser irradiation[16], glass-bead abrasion technique[17], and mechanical abrasion. Mechanical surface treatments like grit blasting or sandpaper are categorised as methods that enhance mechanical interlocking by elevating surface roughness[18]. The manual sanding process using sandpaper is widely used in several studies to treat composite joint surfaces[19–27]. In addition, grit blasting treatment was also used to roughen the composite surface in several studies[28–31]. Meanwhile, several studies have compared several surface treatments such as sanding and grit blasting[32], non-grit and grit blasting[33], plasma treatment and silicon carbide paper[12], sanding and CO_2 laser irradiation[16], and sanding-grit blasting-peel ply treatment[34]. Another study compared the effect of sandpaper grit size from the manual sanding process used on composite joints[35].

Compared with other chemical surface treatments, mechanical treatment provides an extended effect. However, it is extremely labour-intensive and produces significant quantities of waste, notably when the adhesion area is large. Furthermore, residual contamination will likely produce undesirable effects on the combined adherend. Further postprocessing is required following the manufacture of composite materials for surface treatment methods listed below, which may increase overall production costs[36].

The adhesive bonded joint comprises the substrate, the bonding layer, and the interface between substrates and adhesives. To improve the bond strength of joints, enhance the interface for specific substrates and adhesives [37,38]. In addition, surface characteristics such as surface free energy, surface topography, and substrate hardness are extensively associated with the interfaces between substrates and adhesives. A material's surface free energy is an important parameter of surface characteristics and plays an important role in adhesion, adsorption, and wettability[39]. Furthermore, the mechanical interlocking theory states that the cured adhesive forms a meshing connection with the irregular topography of the substrate surface as soon as it fills the gap in the substrate surface[40]. Moreover, it has been found that surface roughness also affects the impact of mechanical interlocking. Subsequently, the bonding strength has been improved[41].

An easy and effective method of achieving desirable surface properties is the mechanical treatment of surfaces with sandpaper. The study from Dehaghani et al. presented that surface treatment using sandpaper resulted in higher joint strength than grit blasting treatment[32]. Depending on the number of sandpaper mesh particles, this treatment may result in various surface roughness and can provide a suitable surface texture while also controlling the sanding direction. However, until now, specialised research has rarely been conducted on the influences of abrasive preparation concerning the adhesive performance of composite joints (grit size and direction of grinding)[35]. Boutar et al. investigated the influence of surface roughness and wettability on the single-lap joint strength of aluminium. They found that the smaller the surface roughness, the better the bond performance. However, carbon fibre laminates are anisotropic materials different from aluminium; therefore, results from literature reports can be used as a reference but may not be exhaustively applied to laminated composites[42].

The objective of this study was to evaluate the adhesion quality of Glass Fibre Reinforced Polymer (GFRP) composite joints, comparing untreated specimens to those sanded with various grit sizes. It focused on how the surface roughness of e-glass fibre/vinyl ester GFRP adherends affected the tensile properties of single lap joints. Specimens were prepared using sandpaper grits of 100, 400, 800, 1200, and a non-grit condition. Surface characteristics such as roughness, morphology, contact angle, and fracture surfaces were analysed to understand the impact of surface treatment on joint tensile strength. Additionally, the Finite Element Method (FEM) was applied to predict fracture locations and stress distributions in the composite joints.

2. Materials and Methods

The method employed in this study adheres to the flowchart depicted in Fig. 1. The Blue section (Part 2.1) of Fig. 1 delineates the VARI process for fabricating composite panels and sectioning them into adherends and test specimens. Part 2.2 portrays the process of sanding treatment for the composites. The purple section of Fig. 1 depicts the specimen preparation for conducting tests on surface roughness (2.3), AFM analysis (2.4), and measuring liquid contact angle (2.5). The green section illustrates the adhesives, fabrication of rigid plastic specimens (2.6), preparation of single lap joint specimens, conducting specimen tests (2.7), simulation procedures (2.9), and SEM analysis (2.8). Detailed explanations of each step depicted in Fig. 1 will be provided in the subsequent subsections.

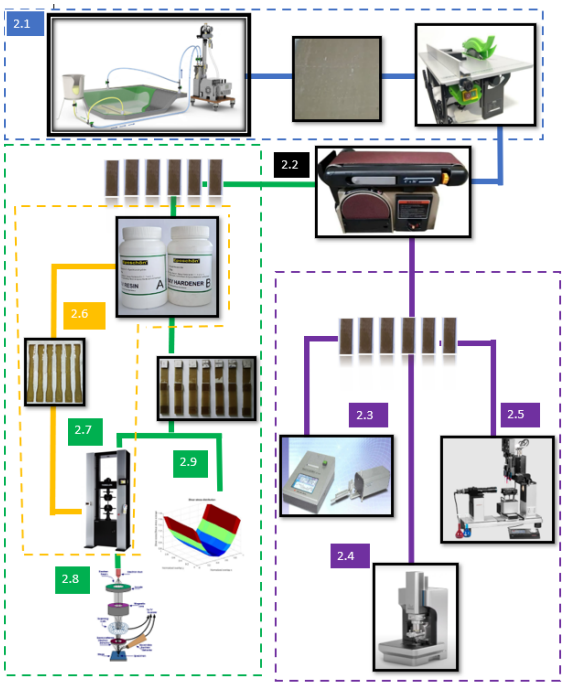

Fig. 1: Flow chart of the study

2.1 Materials and composite fabrication

The adherends were constructed from GFRP composite, incorporating e-glass woven fabric EW-200 as reinforcement and vinyl ester resin as the matrix. This study employed 200 gsm e-glass fibre cloth and utilized Ripoxy R-800 EX-VI vinyl ester resin in a vacuum-assisted resin infusion process. The curing of the vinyl ester resins was facilitated by the cobalt solution P-EX and cumene hydroperoxide solution Percumyl-H, which served as promoters and catalysts. Fibre, resin, promoter, and catalyst can be seen in Fig. 2. Manufacturing the composites required consumables like release agents, tapes (paper and sealant), peel ply, flow media, plastic bagging, and resin delivery systems (hoses, T-connectors, pots, stirrers), alongside the core materials. A two-component epoxy resin, bisphenol A/B, served as the adhesive. All materials were sourced from Justus Kimia Raya Indonesia.

Fig. 2: Glass fabric (a), vinyl ester resin (b), cobalt solution (c), and cumene hydroperoxide solution (d).

Fibre-reinforced polymers were produced using the Vacuum-Assisted Resin Infusion (VARI) process, involving a setup that included a flat glass mould, fibre lamination, peel ply, flow mesh, vacuum bag, sealant tape, resin inlet and outlet, and a vacuum pump as illustrated in Fig. 3. The composites comprised 18 layers of e-glass fabric, with the vinyl ester resin mixture containing 0.3% promoter and 1% catalyst by mass. The fibre-to-resin mass ratio in the VARI process was approximately 70:30.

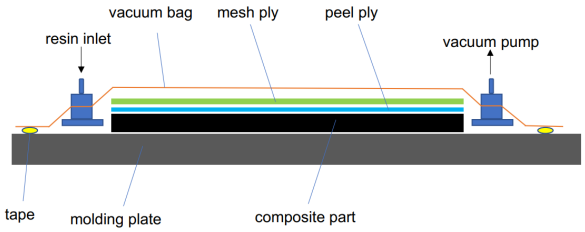

Fig. 3: VARI illustration.

The VARI process employed a vacuum pump to spread resin across the laminated fibre area. Initially, dry fibres were laid on the mould surface, then covered with peel ply, mesh ply, and a vacuum bag. A vacuum was then applied to remove air from the bag, and upon achieving a vacuum state, the resin was infused through the inlet duct into the laminate until full saturation was reached (see Fig. 4). The vacuum was maintained until the resin gelled, utilizing a 100 kPa pressure from a Vacmobile vacuum pump. The composite panels were then left to cure at room temperature for 24 hours.

The adherends were produced by cutting composite panels to the dimensions specified in ASTM D5868, using a diamond circular table saw at 2950 rpm. Each adherend measured 3 mm in thickness, 101.6 mm in length, and 25.4 mm in width. A total of 70 composite panel adherends were fashioned into specimens, with every two adherends forming one specimen.

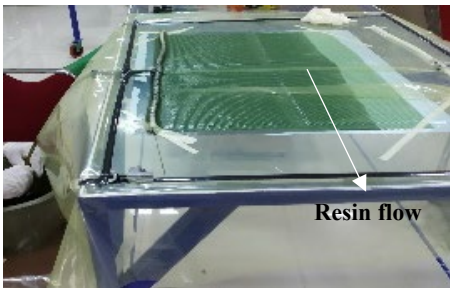

Fig. 4: Composite fabrication.

Tabs for the specimens were crafted from the same materials and through identical processes as the adherends, cut from 25.4 mm by 25.4 mm composite panels. Two tabs were attached to each specimen, one at each end.

2.2 Abrasive treatment

The composite adherends were divided into five groups, each containing 7 specimens (14 adherends per group). Each group received abrasive surface treatment with a 100 mm x 915 mm sandpaper belt of varying grit sizes, detailed in Table 1. The first group served as the untreated reference. Groups two to five were sanded with sandpaper belts of grit sizes 100, 400, 800, and 1200, respectively.

Table 1. Abrasive treatment.

Group	Surface treatment	Grit size
1	None	-
2	Sanding	Grit 100 sandpaper belt
3	Sanding	Grit 400 sandpaper belt
4	Sanding	Grit 800 sandpaper belt
5	Sanding	Grit 1200 sandpaper belt

The sanding process utilised a Rockwell belt sander set at 1700 fpm. Adherends in groups two to five were sanded on the adhesive side to match the overlap area of one inch (25.4 mm). Post-sanding, the surfaces were cleansed with acetone to eliminate any residues. This procedure was applied to all adherends destined for further analyses such as Atomic Force Microscopy (AFM), surface roughness, and liquid contact angle measurements, as well as for those used in single lap adhesion joint tests. The difference between treated and untreated surfaces is illustrated in Fig. 5.

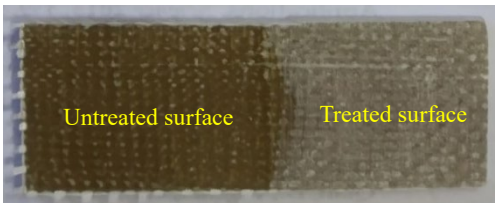

Fig. 5: The treated and untreated surface of the composite.

2.3 Surface roughness analysis

Surface roughness was assessed on both treated and untreated adherend surfaces across all groups to ascertain the roughness values. This analysis involved calculating the arithmetic mean roughness (Ra) value, conducted with the SE 300 Surface Roughness Tester. For each of the five specimens listed in Table 1, three measurements were taken. This analysis was conducted at the Advanced Characterization Laboratory I Metallurgy, BRIN.

2.4 Atomic force microscope (AFM) analysis

One of the most effective interpretation methods for the structural and morphological examination of polymeric composites is atomic force microscopy (AFM)[43]. Three-dimensional morphologic images with resolutions in the nanometre range can be generated with AFM[43]. AFM analysis was carried out on both treated and untreated adherend surfaces across all groups to examine the composite's surface morphology, using the AFM Park NX10 machine. This analysis, conducted in the same laboratory as the surface roughness assessment, is depicted in Fig. 6. The results enable the generation of three-dimensional (3D) topographic images with nanometre-scale resolutions.

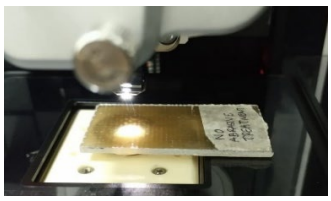

Fig. 6: AFM analysis.

2.5 Liquid contact angle analysis

The liquid contact angle assessment, which evaluates the angle formed between a liquid and a solid surface, was conducted to determine the wettability, hydrophobicity, and hydrophilicity of both treated and untreated adherend surfaces, thereby assessing liquid absorption. This testing used an OCA 25 machine, as depicted in Fig. 7. It was conducted at UPT Laboratory Diponegoro University.

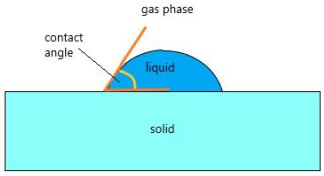

Fig. 7: Liquid contact angle.

2.6 Tensile test of adhesives

Tensile tests were performed on the epoxy adhesive used in this study to evaluate its tensile properties, with adjustments made to the hardener composition to identify the ideal resin-to-hardener ratio. Three ratios were tested: 1:1, 2:1, and 1:1.5, each with five rigid plastic specimens in a dog bone shape, conforming to ASTM D638 standards, as illustrated in Fig. 8. The specimens were tested to failure using a Tensilon universal testing machine. The ratio with the best tensile properties was selected for the adhesive in single-lap joint specimens and provided material parameters for composite joint simulations.

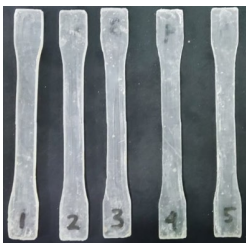

Fig. 4: Epoxy adhesive specimens.

2.7 Single lap shear joint test (SLJ)

Adherends, both treated and untreated, were assembled into single lap joint (SLJ) specimens at room temperature, grouped as per Table 1, using an epoxy adhesive A/B mix with the best resin-to-hardener ratio. Each SLJ specimen comprised two adherends bonded over a 25.4 mm area. For groups 2-5, this area was pre-treated by sanding with specified sandpaper grits, whereas for group 1, the adherends were bonded at unsanded surfaces.

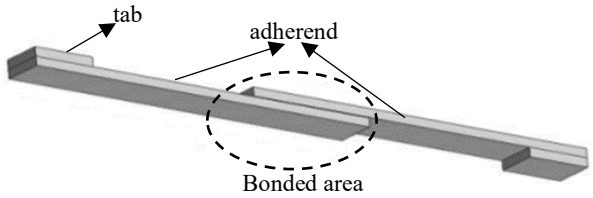

Fig. 9: Single lap joint specimen.

The epoxy adhesive was homogeneously mixed with the catalyst for 2 minutes, applied to assemble the adherend surfaces, and secured using paper clips. Excess adhesive in the bonded area was removed with a dry cloth. The bonded area of the SLJ specimen can be seen in Fig. 10. Specimens were left at room temperature for 24 hours for complete curing of the adhesive. Subsequently, tabs were affixed to both ends of the specimen similarly. The two tabs are installed crosswise, as shown in Fig. 9, ensuring that the loading during testing is directly applied to the specimen. Specimens were stored in a dry cabinet with a temperature of 23 ± 2 ^{0}C and a humidity of 50 ± 5%.

The test of single-lap shear adhesion was carried out to determine the maximum load capacity of the composite joints. This test was performed on sanded and unsanded composite specimens from Rockwell belt sanding machines with sandpaper belt's grit size variations of 100, 400, 800, and 1200. The tests were conducted at the Materials Testing Laboratory, Research Centre of Aeronautics Technology, ORPA, BRIN.

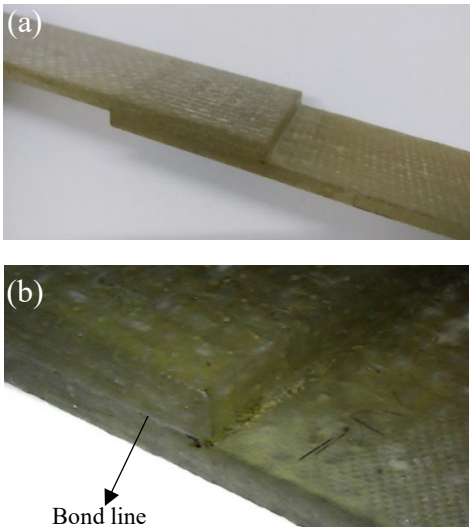

Fig. 10: Bonded area (a) and bond line (b) of SLJ specimen.

The single lap shear adhesion test used a 100 kN Tensilon UTM tool with a constant crosshead speed of 13 mm/minute as per ASTM D5868. Specimens were mounted on UTM by clamping the tabs on the upper and lower jaws. The specimens were tested until they fail or are released at the joints. Load and strength data were recorded using UTM software. Installation of SLJ specimens on UTM during testing can be seen in Fig. 11. The SLJ test was carried out for each group of 7 specimens and 35 specimens for five groups.

Fig. 11: SLJ test.

2.8 SEM (scanning electron microscopy) observations

SEM analysis was carried out to determine the characteristics of the fracture surface in the composite adhesive joint. This analysis was carried out on sanded and unsanded composite specimens. Tests were conducted at the Propellant Laboratory, BRIN, as shown in Fig. 10. Specimens were prepared from damaged samples due to the single lap shear adhesion test. SEM testing is only carried out on loose overlap surfaces.

Fig. 12: Sample observation using SEM.

Specimens were made with dimensions of 5x5 mm for each variation. The number of test specimens consisted of 5 SEM specimens with non-grit variations, grit 100, grit 400, grit 800, and grit 1200. The test focused on the composite's fracture surface areas with the adhesive remains.

2.9 Finite element (FE) modelling

FE modelling was conducted to estimate the shear stress in an adhesive joint. The adherend, comprising a composite plate, was simulated using shell elements, while the adhesive, responsible for bonding two similar adherends, was modelled using spring elements. The analysis adopted a linear static plane stress assumption, particularly applicable when the thickness is substantially smaller than other dimensions in the model. This assumption facilitated a clearer depiction of shear stress within the overlap bonded area in both the x and y directions. However, a 2D plane strain analysis is often preferred in adhesive joints[44].

In determining shear stresses, two types of spring elements were utilised. These spring elements are interconnected by two rigid body elements (RBE) to

simulate the adhesive material, as seen in Fig. 13. Tahmasebi[45] initially introduced this adhesive modelling approach to analyse bonded joints.

The shear stiffness values (k_{si}, k_{se}, k_{sc}) are required to determine shear stress in the x and y direction.

$$k_{si} = \frac{A_a\, G}{t_a} \quad (1)$$

$$k_{se} = \frac{A_a\, G}{2\, t_a} \quad (2)$$

$$k_{sc} = \frac{A_a\, G}{4\, t_a} \quad (3)$$

Where In Eq. 1-3, k_{si} is stiffness value in shear direction for internal element, k_{se} is stiffness value in shear direction for edge element, k_{sc} is stiffness value in the shear direction for the corner element, A_a is the area of the adhesive element, E is the adhesive elastic modulus, G is the adhesive shear modulus, t_a is adhesive thickness, v is Poisson's ratio.

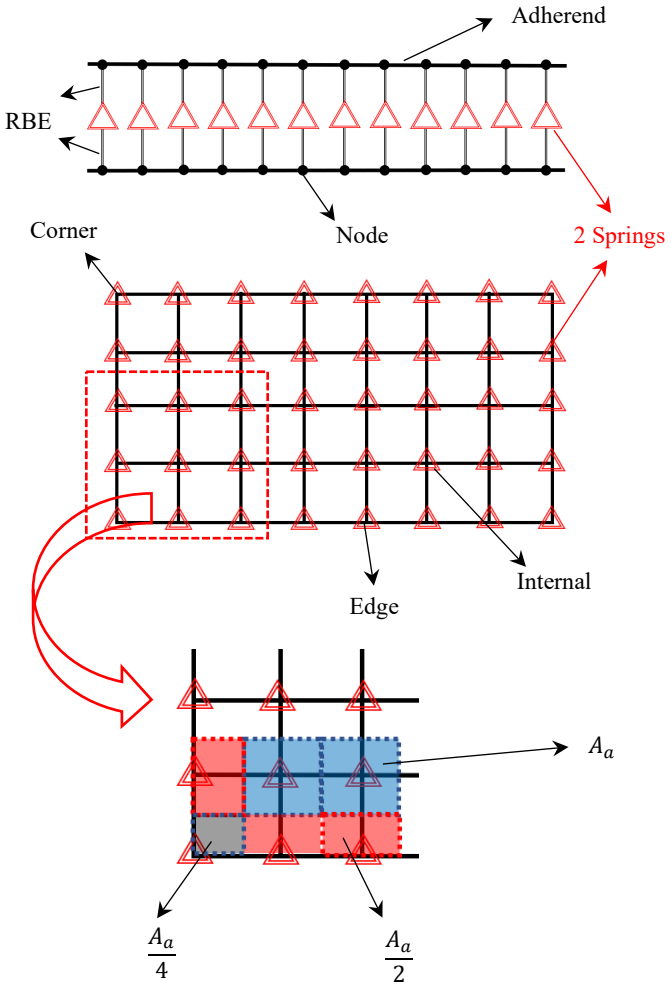

Fig. 13: Adhesive model using spring element. There are two spring elements in each node in the adhesive area. The node location is divided into corner, edge, and internal.

The shear stress in the adhesive joint can be obtained using the formula below.

$$\tau_i = \frac{\sqrt{{f_{x,i}}^2 + {f_{y,i}}^2}}{A_a} \quad (4)$$

Where In Eq. 4, τ_i is the shear stress at node i, A_a is the area of the adhesive element, $f_{x,i}$ is the spring force in the x-direction at node i, $f_{y,i}$ is the spring force in the y-direction at node i.

The model used the material properties of glass/vinyl ester for adherend and epoxy A/B for adhesive, as displayed in Table 2.

Table 2. Mechanical properties of the materials

	Adherend	**Adhesive**
E (MPa)	-	2310
E1 (MPa)	25000	-
E2 (MPa)	25000	-
v12	0.2	0.3

3. Results and Discussion

3.1 Influence of sanding treatment on the quality of composite surface

3.1.1 Surface roughness

Table 3 presents the composite arithmetic average of Ra (roughness profile) evaluation results. The initial Ra of the test object's surface was 0.21 ± 0.02 µm. Post-sanding treatments with grit 100, 400, 800, and 1200 resulted in Ra values of 4.16 ± 0.51, 2.00 ± 0.13, 1.46 ± 0.15, and 1.29 ± 0.17 µm, respectively. These results indicate an increase in surface roughness after each sanding treatment. Notably, specimens treated with grit 100 sandpaper belt exhibited the highest Ra (4.16 ± 0.51 µm), while non-treated specimens showed the lowest Ra (0.21 ± 0.02 µm). The measured non-treated surface roughness pertains to the composite surface attached to the glass mould, highlighting the significant influence of the mould or media in the VARI composite manufacturing process.

Table 3. Arithmetic average of roughness profile (Ra) for treated and non-treated composite

Sandpaper grit	**Ra (µm)**
None	0.21 ± 0.02
1200	1.29 ± 0.17
800	1.46 ± 0.15
400	2.00 ± 0.13
100	4.16 ± 0.51

Figure 14 illustrates the comparison of surface roughness between non-treated and treated glass/vinyl ester composites. The analysis indicates that as the grit value of the sandpaper increases, the surface roughness value decreases, as depicted in Fig. 14. Similar results were reported by Yang et al.[35]. Compared to the non-

treated, grit 400, grit 800, and grit 1200 specimens, those treated with grit 100 showed a higher standard deviation of Ra It indicates that grit 100 produced a non-homogeneous surface topography.

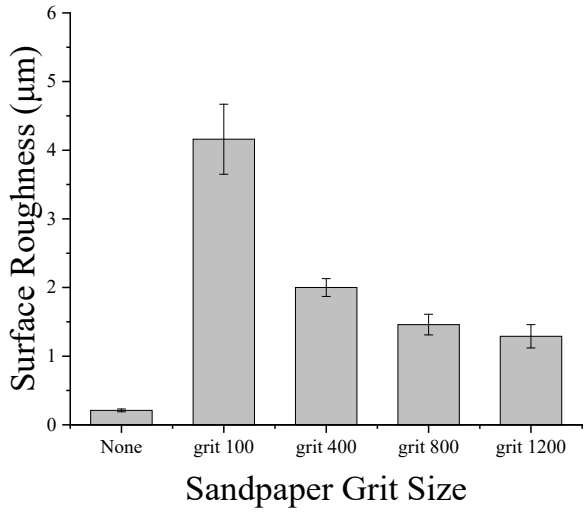

Fig. 14: The surface roughness of glass/vinyl ester specimen.

3.1.2. Surface morphology

AFM microscopy enables the examination of material morphology and surface characteristics down to the atomic level Fig. 15 shows the surface morphology of the data obtained via atomic force microscopy. According to the results, the morphology and texture of the composite changed depending on the sandpaper grit used. The morphology of the untreated specimen is an epoxy surface (Fig. 13(a)), which is the surface that adheres to the flat glass mould during composite fabrication. The AFM photographs showed a uniform surface in almost all surface areas of the untreated specimens. The morphology of the non-treated surface differed from that of the sand-treated surfaces. The treated specimens exhibited a morphology resembling hills with peaks, although this appearance varied with each grit treatment. The peaks on the surface of the grit 800 specimen appear uniform across the entire surface area, as depicted in Fig. 15(d). Among the specimens, grit 800 exhibited the most uniform peaks, followed by grit 100 (Fig. 15(b)), grit 400 (Fig. 15(c)), and grit 1200 (Fig. 15(e)), in descending order. AFM analysis showed that the specimens with the grit 800 sand paper belt treatment had the most uniform surface morphology. The peaks on the grit 800 specimens appear smaller and evenly distributed, as shown in Fig. 15(d). The peaks on the grit 100 and 400 specimens appeared larger than those on the grit 800 specimens, but their distribution was uneven, only occurring in a few locations, while on other surfaces, they were not visible. Meanwhile, on the surface of the grit 1200 specimen, the peak appeared lower than other treated specimens and tended to be flat in some areas. The surface of the 1200 grit specimen is indicated to be smoother than other grits, according to the previous discussion on surface roughness results.

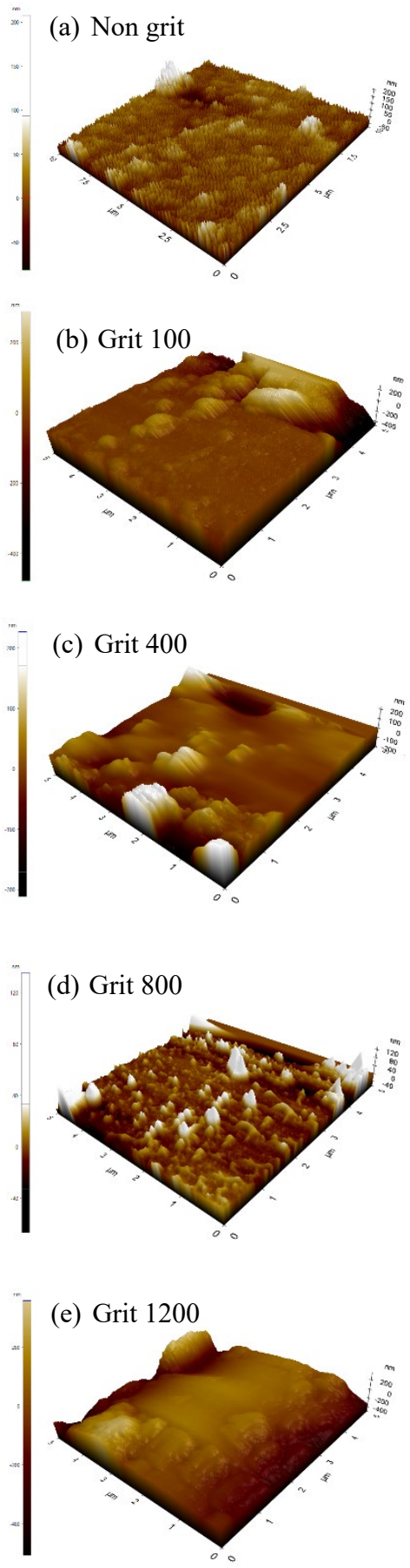

Fig. 15: AFM micrographs of the composite specimen.

3.1.3. Contact angle

Table 4, Fig. 16, and Fig. 17 display the composite contact angle measurement results. The liquid contact angle of the untreated specimen surface was measured at 125.3 ± 1.6° (Fig. 17(a) and Table 4). The high contact angle indicates that the surface of the untreated specimen (vinyl ester surface) is near-super-hydrophobic. The study of Ramaswamy et al. reported similar results[33]. However, the value of this surface contact angle decreased after the sanding treatment using a variety of grit sandpaper belts. The contact angles reduced to 109.0 ± 1.4°, 102.4 ± 2.2°, 97.2 ± 1.0°, and 103.3 ± 1.7° on the grit 100, grit 400, grit 800, and grit 1200 composite specimens, respectively. It is obvious that when grit sizes rise, the surface contact angles of the specimens tend to gradually decrease and then increase with the grit size increase, as can be seen in Fig. 16. In other words, the surface roughness of the composite influences the wettability of the specimen surface. Similar results were reported by Yang et al.[35].

The decrease in the contact angle value could be related to fibre exposure due to the sanding process[46]. Even though there is a decrease, the value still indicates that the specimen is hydrophobic due to a contact angle of more than 90°. The reduction in liquid contact angle treated specimens was 13%, 18%, 22%, and 18% for specimens with grit sizes of 100, 400, 800, and 1200, respectively. Similar to the arithmetic average of the roughness profile, the liquid contact angles varied according to the grit of the sandpaper used for the sanding. Specimens treated with grit 800 sandpaper belts produced the lowest contact angle of 97.2 ± 1.0° (Fig. 17(d)).

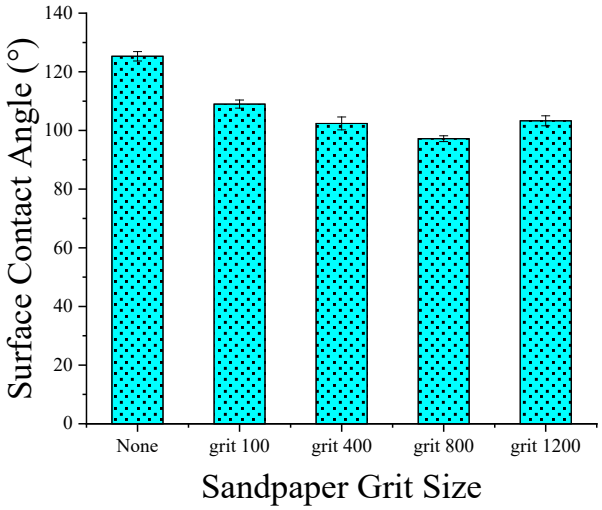

Fig. 16: The surface contact angle of the glass/vinyl ester specimen.

Surface roughness had an impact on the specimens' wettability[35]. A lower contact angle value indicates greater wetting and adhesion characteristics of the materials[12]. Due to the smaller contact angle, the treated composite will have better wettability and adhesion properties than the untreated composite. Hence, according to the results, the grit 800 composite specimen will have better wetting and adhesion characteristics than other specimens. However, the differences in these characteristics between untreated specimens are unlikely to be significantly different because the difference value is only 5% to 12% compared to the grit 800 specimens.

Table 4. Liquid contact angle for treated and non-treated composite.

Sandpaper grit	**Θ (°)**
None	125.3 ± 1.6
1200	103.3 ± 1.7
800	97.2 ± 1.0
400	102.4 ± 2.2
100	109.0 ± 1.4

Figure 17 exhibits liquid droplets on the surface of the composite specimen. All the droplets in Fig. 17 form an obtuse angle to the composite surface, indicating the specimen surface's hydrophobicity.

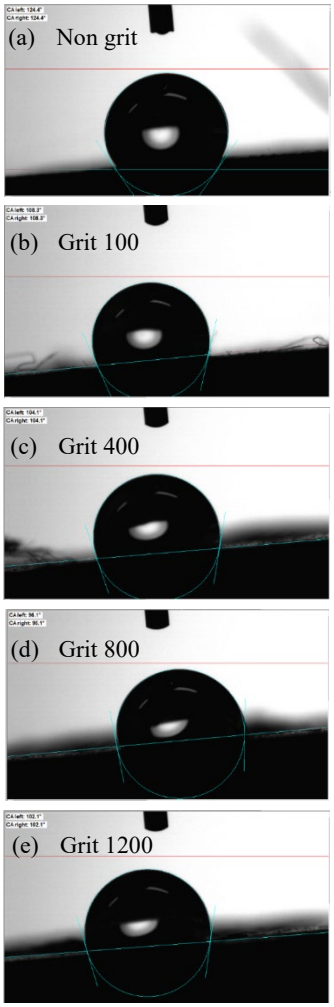

Fig. 17: Liquid contact angle of the liquid droplet on the composite specimen.

3.2 Tensile properties of adhesive

Figure 18 illustrates stress vs. strain curves of epoxy adhesives with varying resin-to-hardener ratios. These curves exhibit distinct ultimate strength and tensile modulus values. The epoxy adhesive specimens with a resin-to-hardener ratio of 2:1 demonstrated the highest tensile strength and modulus values, followed by specimens with ratios of 1:1 and 1:1.5, respectively. Specifically, the tensile strength and modulus values for the epoxy 2:1 ratio were 37.89 ± 4.26 MPa and 2.31 ± 0.23 GPa. For the 1:1 ratio, the tensile strength and modulus values were 21.20 ± 3.43 MPa and 1.10 ± 0.11 GPa, respectively. Meanwhile, the epoxy 1:1.5 ratio exhibited tensile strength and modulus values of 13.16 ± 1.18 MPa and 0.62 ± 0.19 GPa, respectively. Hence, the optimal epoxy resin-to-hardener ratio is determined to be 2:1. This ratio was utilised as an adhesive for Single Lap Joint (SLJ) specimens, and its property values were subsequently employed in the simulation of Glass Fibre-Reinforced Polymer (GFRP) adhesive joints.

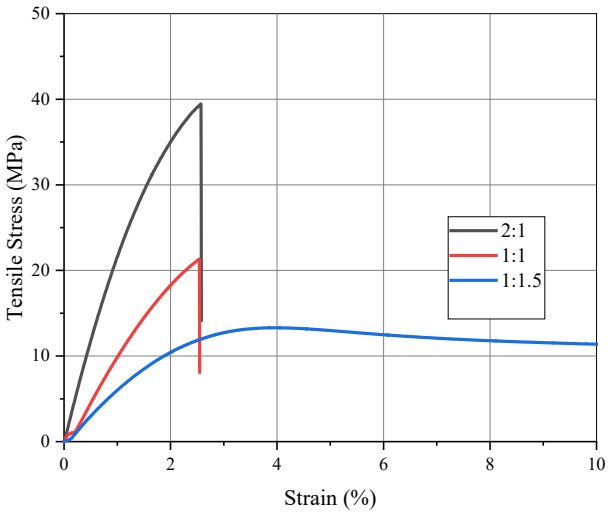

Fig. 5: Stress-strain curves of epoxy adhesive.

3.3 Effect of sanding treatment on single lap shear joint strength of composite

Figure 19 displays the stress vs. strain curves of untreated and treated composite joints. The five groups of specimens show similar curves consisting of two different slopes. The first slope was 0 to 0.2% strain, where all curves had nearly the same slope and coincide. The second slope was in the area after 0.2% strain until the specimen experienced final failure, marked by a dropping curve. Unlike the first slope, the second slope differed for each specimen; only the grit 400 and 1200 specimens had similar slopes. The peak curve for treated specimens was higher than for untreated specimens. These results illustrate that the sanding process increases the adhesive joint shear strength of the specimen.

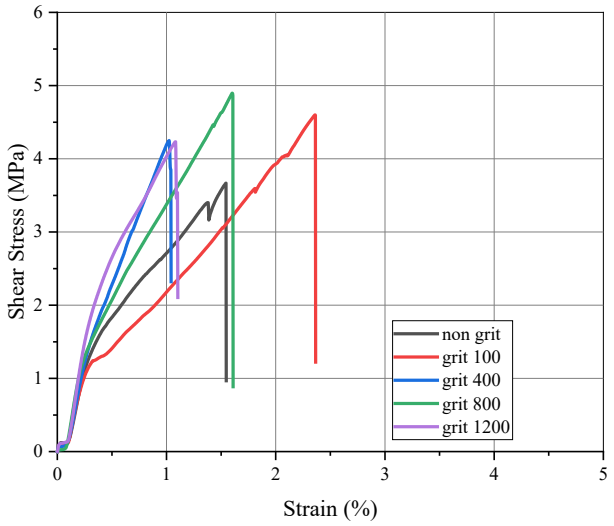

Fig. 19: Stress-strain curves of glass/vinyl ester bonded joints.

Figure 20 and Table 5 summarise the single lap shear joint test results. Figure 20 illustrates that surface treatment with sanding can increase the composite's adhesive joints' shear strength, although the value of the increase differs depending on the grit size of the sandpaper used. Table 5 displays composite adhesive joints' shear strength values after SLJ testing. The lap shear strength of the untreated composite was 3.53 ± 0.65 MPa. Meanwhile, the lap shear strength of treated composites was 4.20 ± 0.70 MPa, 4.85 ± 0.24 MPa, 4.22 ± 0.28 MPa, and 4.60 ± 0.33 MPa for grit 1200, grit 800, grit 400, and grit 100 specimens, respectively. According to these results, the lap shear strength of the glass/vinyl ester adhesive joint increased after sanding treatment. It can be related to the sanding process, which exposes glass fibres on the surface of the specimen and bonds them with the epoxy adhesive. Thus, the increase in lap shear strength can be attributed to better chemical compatibility between glass fibre and epoxy adhesive than between vinyl ester and adhesive. Similar results were declared by Sorrentino et al.[34] and Bechikh et al.[46].

After sanding treatment, specimens showed an increase in adhesion strength by about 19% to 37% compared to untreated specimens. The highest increase was in the grit 800 specimens, which showed the best shear strength compared to other treated specimens. It relates to uniform surface topography analysis results and the lowest contact angle values. This characteristic causes the grit 800 specimens to have good wettability and adhesion characteristics to the adhesive, resulting in the best shear strength. Meanwhile, the shear strength values of grit 400 and 1200 composites tended to be similar and only differed by 0.5%. It is related to similar contact angle values, which indicate similar wettability and adhesion properties to the adhesive, which means the mechanical strength is also similar. However, compared to the grit 800 specimens, the shear strength of the other treated

specimens was lower by 5% for the grit 100 specimens and 13% for the grit 400 and 1200 specimens.

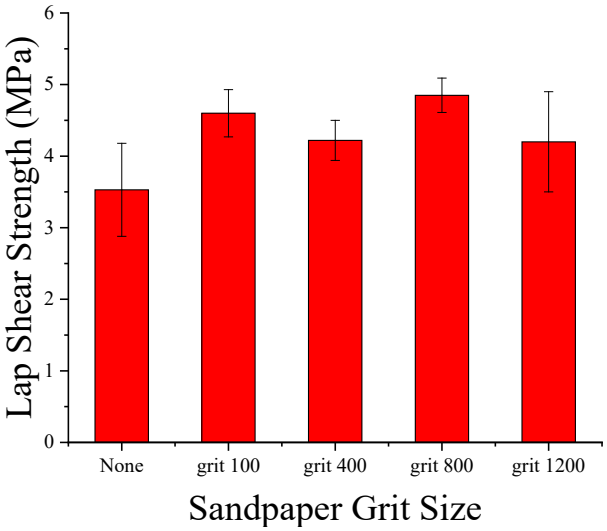

Fig. 20: Lap shear strength comparison of glass/vinyl ester composites.

Table 5. Results of a single lap shear joint test on treated and untreated glass/vinyl ester composite.

Sandpaper grit	Lap shear strength (MPa)	Deviation/ref
None	3.53 ± 0.65	ref
1200	4.20 ± 0.70	+19%
800	4.85 ± 0.24	+37%
400	4.22 ± 0.28	+20%
100	4.60 ± 0.33	+30%

Figure 21 shows the fracture surface of the bonded area after single lap shear joint testing for treated and non-treated composites. Figure 21(a) illustrates the fracture in non-treated composites in the adhesive fracture mode. The fracture occurred at the adhesive/adherend interface, characterised by the adhesive sticking only to the right surface and the left surface showing no adhesive sticking (Fig. 21(a)). The adherend surface on the left only shows a composite surface that is clean of adhesive, which indicates that the adhesive is completely released from this surface after the SLJ test. Treated specimens show a mixed-mode fracture, as shown in Fig. 21(b)-(e). The fracture modes that occur are cohesive and adhesive. The fracture occurs in the adhesive, indicating a cohesive fracture mode. Then, one part of the fracture detaches from the adherend and adheres to the other, showing adhesive fracture mode. These two fracture modes are visible on the treated specimen surface in Fig. 21(b)-(e).

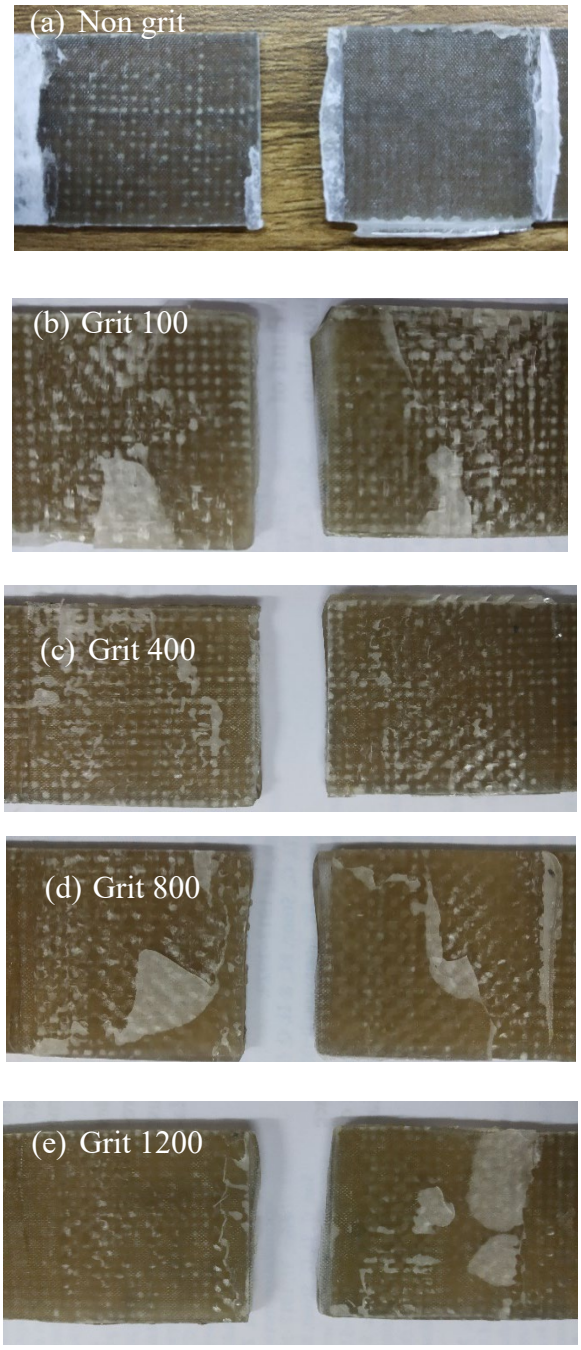

Fig. 21: Fracture surface of the bonded area after SLJ test.

3.3. SEM

Figure 22 and 23 show the results of the SEM photo of the fracture surface of the specimen after the SLJ test. The results of the SEM micrograph of the GFRP composite joints were in the form of fracture surface images of the test specimens. The SEM results show that the adhesive of a non-treated composite joint is detached on one side of the adherend because the surface is smoother. It is evident from the SEM photo, which shows the woven e-glass fibre, which is visible on the surface of the SEM photo, as shown in Fig. 19. The clear appearance of the fibre

bundles in Fig. 19 illustrates that the adhesive was completely removed from the surface of the untreated specimen. It is the evidence that the failure in this specimen occurred at the adhesive/adherend interface.

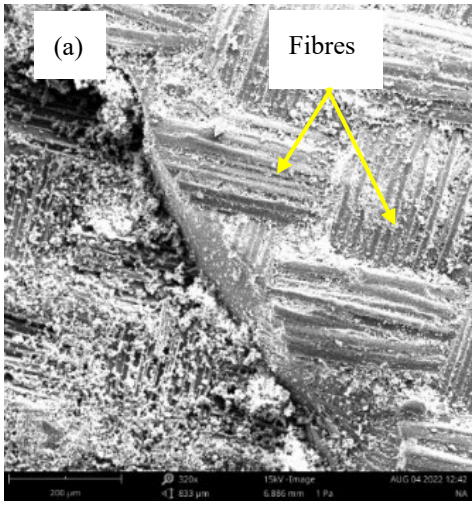

Fig. 22: SEM micrographs of untreated specimen fracture surface.

Figure 23(a)-(d) illustrates the micrograph results of the fracture surface of the sanded specimen after the single lap joint test. SEM micrographs were taken of the adhesive fracture area. The previous discussion stated that in sanded specimens, mix-mode failure occurred. The failures that appear are cohesive failure modes or fracture on the adhesive and adhesive failure modes or fracture on the adherend/adhesive interface. These two failure modes are clearly illustrated in Fig. 23(a)-(d). The occurrence of cohesive and adhesive failures was characterised by residual adhesive in both released adherends. It is illustrated by the broken adhesive layer on top of the adherend (cohesive failure mode), while the remaining adhesive breaks are not attached to the adherend underneath, as illustrated in Fig. 23(a). In other words, the remaining adhesive breaks off from the adherend and attaches to another adherend (adhesive failure mode). It is visible in Fig. 23(b)-(e), especially in Fig. 23(a).

Figure 23(b)-(d) shows the presence of fibre fractures on the fracture surface of the sanded specimen. It proves that the sanding has exposed the fibre to the adherend surface. Fibres exposed on the adherend surface will be bound by the adhesive and break when they fail after the single lap joint test. It also proves that the chemical compatibility between fibre and epoxy adhesive is better than between epoxy adhesive and vinyl ester resin, causing the shear strength of sanded specimens to be better, as discussed previously. This bond between the adhesive and the fibre is also evident from the fibre imprint on the adhesive fracture surface in Fig. 23(c). Fibre imprint failure occurs due to the release of the fibre and polymer bonds after mechanical testing.

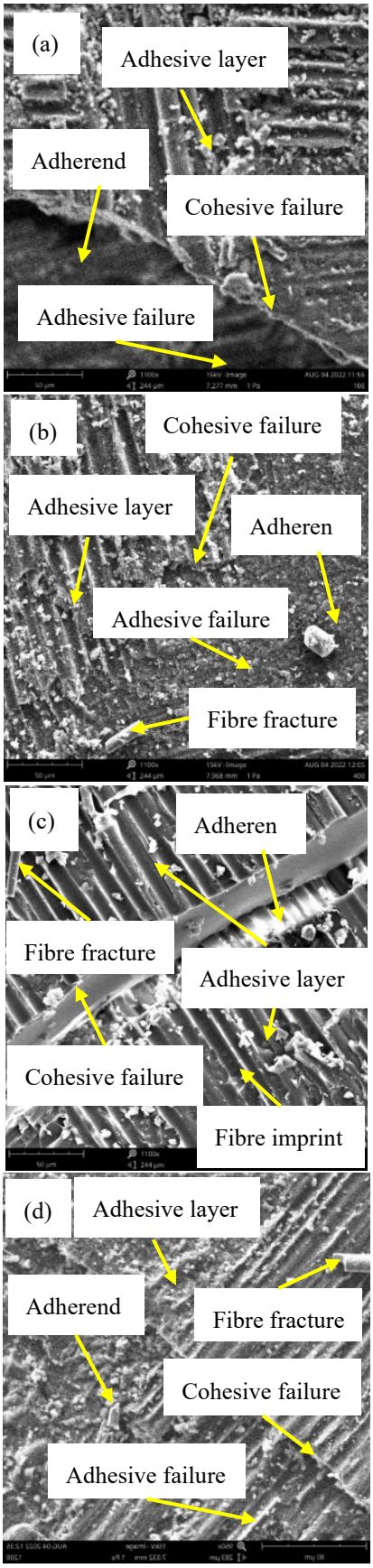

Fig. 23: SEM micrographs of specimen fracture surface: (a) grit 100, (b) grit 400, (c) grit 800, (d) grit 1200.

3.3 Finite element (FE) results

The finite element model was used to predict the shear stress that occurred in the adhesive joint. The finite element modelling employed the assumption of linear static plane stress.

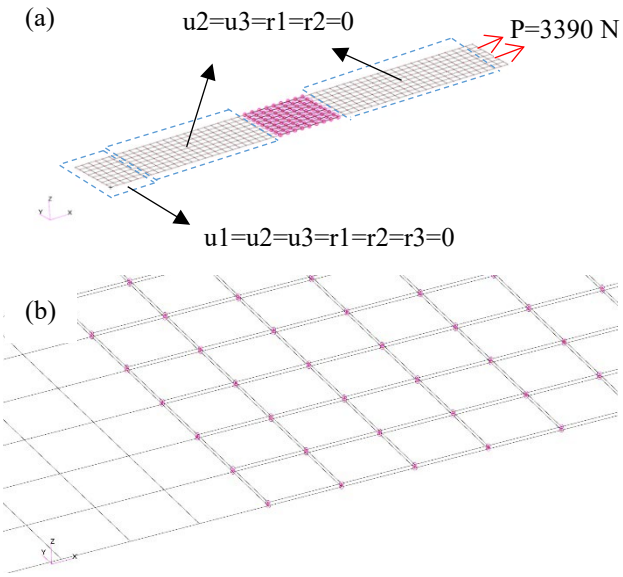

Fig. 24: Finite element model: (a) SLJ specimen, (b) adhesive joint.

Figure 24 is a finite element model of the SLJ specimen, consisting of shell elements, spring elements, and Rigid Body Elements (RBE). There was a total of 528 shell elements, 243 spring elements, and 162 RBE in the model.

The SLJ was subjected to load in the x-direction at the tip of the specimen. The lower tab was constrained in the translation and rotation of x, y, and z. Other nodes shown in Fig. 25 are able to translate in the x and y direction and rotate in the z direction.

The adhesive joint was modelled using spring elements connecting the two adherends. Therefore, shear stress distribution in the adhesive joint could be observed.

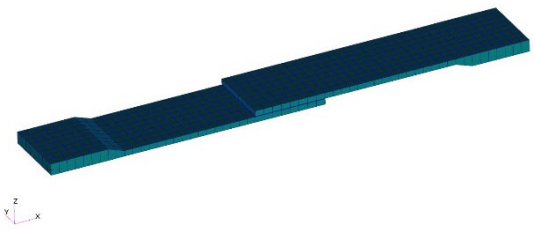

Fig. 25: 3D view to verify the SLJ model.

Figure 25 shows a 3D view of the finite element model used for finite element modelling geometry verification. The 3D view model was constructed by displaying the 2D finite element thickness. The model was then compared to the geometry of the SLJ specimen for verification. The most critical aspect of consideration during the modelling was the gap between the adherends, which determined the thickness of the adhesive.

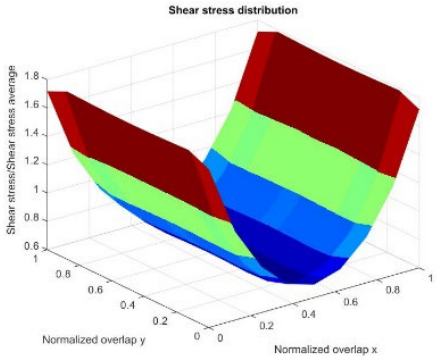

Fig. 26: Shear stress distribution in an adhesive joint of the single lap joint specimen subjected to 3390 N load.

The shear stress distribution within the adhesive joint was determined using finite element analysis, with the adhesive joint being modelled using spring elements. Shear stress was calculated based on the forces acting on the springs in the x and y directions at the locations of these spring elements. Spring elements offer advantages such as simplicity, computational efficiency, broad applicability, ease of interpretation, and suitability for initial design assessments but they may not fully capture the complexity of adhesive behaviour compared to cohesive elements, which provide a more detailed and accurate representation.

Figure 26 illustrates the shear stress over the average shear stress distribution in the adhesive joint. The graph exhibits a U-shaped curve, with the minimum value occurring at the midpoint (x=0.5) and maximum values observed at the edges (x=0 and x=1). Specifically, the minimum value was 0.635, and the maximum value was 1.785. Corners tend to have lower values compared to the maximum values at the edges. Furthermore, various single lap theories provide maximum values ranging from 1.94 to 2.91[47]. To achieve better results, it is necessary to use finer elements, especially in the bonded area.

Based on single lap joint tests, there's variation in the shear strength of both the untreated and treated composites with different grits. The average shear stress in the bonded area under a load of 3390 N was 5.25 MPa. However, this value varies among several test results, likely due to differences in either the mechanical properties of the adhesive material or the dimensions in each specimen configuration. The discrepancy in shear stress ranges from 7.62% to 32.76%.

4. Conclusions

The influence of sanding treatment with variation of sandpaper belt grit sizes on the lap shear strength of Gass Fibre-reinforced Polymer (GFRP) adhesively bonded Single Lap Joints (SLJ) was evaluated in this work. Adherends were cut from GFRP composite panels that

were made by a vacuum-assisted resin infusion process. Sanding was treated using a belt sander machine with sandpaper grit size variations of 100, 400, 800, and 1200.

The results of the surface roughness analysis showed that the higher the grit value of the sandpaper used, the smaller or finer the surface roughness value. Specimens treated with grit 100 sandpaper belt produced the highest Ra (4.16 ± 0.51 μm), and specimens non-treated produced the lowest Ra (0.21 ± 0.02 μm).

Sanding treatment increased the surface roughness of the composite specimens. Sanding treatment increased lap shear strength by 19% to 37% compared to the untreated specimens.

The sanding treatment exposes the fibres to the surface of the specimen, facilitating a direct bond between the adhesive and the fibres. This direct bond between the fibre and epoxy adhesive yields superior bonding compared to that between vinyl ester and epoxy adhesive. SEM micrograph illustrates this bond, characterised by fibre breaks on the fracture surface of the GFRP.

However, shear strength does not solely depend on surface roughness. The abrasion treatment utilizing a grit 800 sandpaper belt produces SLJ specimens with the highest shear strength. AFM analysis found that the specimens treated with the grit 800 sandpaper belt had the most uniform surface morphology. The peaks on the grit 800 specimens appear smaller and evenly distributed than those with other grit sizes. Thus, it results in a lower contact angle on the grit 800 than different grit sizes, which means better wettability and adhesion properties. Therefore, surface morphology is the parameter that most influences shear strength, resulting in a lower contact angle.

The shear stress in the bonded area under a load of 3390 N is 5.25 MPa. However, this value varies among several test results, likely due to differences in either the mechanical properties of the adhesive material or the dimensions in each specimen configuration. The discrepancy in shear stress ranges from 7.62% to 32.76%.

Based on the finite element result, the minimum value of shear stress over the average shear stress in the adhesive joint, occurring at the midpoint (x=0.5) and maximum values observed at the edges (x=0 and x=1). Specifically, the minimum value was 0.635, and the maximum was 1.785.

Acknowledgements

The authors acknowledge the research funding support from “Organisasi Riset Penerbangan dan Antariksa”, No. 28/III.1/HK/2023 by the National Research and Innovation Agency - BRIN, the Republic of Indonesia.

References

1) M.K. Gupta, V. Singhal, and N.S. Rajput, “Applications and challenges of carbon-fibres reinforced composites: a review,” *Evergreen*, 9 (*3*) 682–693 (2022). doi:10.5109/4843099.
2) S.W. Park, and D.G. Lee, “Adhesion characteristics of carbon black embedded glass/epoxy composite,” *J. Adhes. Sci. Technol.*, 24 (*4*) 755–773 (2010). doi:10.1163/016942409X12579497420807.
3) N.K. Yadav, N.S. Rajput, S. Kulshreshtha, and M.K. Gupta, “Investigation of the mechanical and wear properties of epoxy resin composite (ercs) made with nano particle tio2 and cotton fiber reinforcement,” *Evergreen*, 10 (*1*) 63–77 (2023). doi:10.5109/6781041.
4) S. Bindu, M.P. Kumar, and K.M. Vinay, “Development and mechanical properties evaluation of basalt-glass hybrid composites,” *Evergreen*, 10 (*03*) 1341–1348 (2023). https://doi.org/10.5109/7151681
5) D. Choudhari, and V. Kakhandki, “Characterization and analysis of mechanical properties of short carbon fiber reinforced polyamide66 composites,” *Evergreen*, 8 (*4*) 768–776 (2021). doi:10.5109/4742120.
6) D.S. Patil, and M.M. Bhoomkar, “Investigation on mechanical behaviour of fiber-reinforced advanced polymer composite materials,” *Evergreen*, 10 (*1*) 55–62 (2023). doi:10.5109/6781040.
7) S. Ray, “Effect of control parameters on erosion wear performance of glass-epoxy composites filled with waste marble powder,” *Evergreen*, 9 (*1*) 23–31 (2022). doi:10.5109/4774213.
8) M. Awi, and A.S. Abdullah, “A review on mechanical properties and response of fibre metal laminate under impact loading (experiment),” *Evergreen*, 10 (*1*) 111–129 (2023). doi:10.5109/6781057.
9) A.J. Kinloch, “Adhesion and Adhesives: Science and Technology,” 1st ed., Cambridge University Press, 1987. doi:10.1007/978-94-015-7764-9.
10) A. Sharma, H. Chawla, and K. Srinivas, “Prediction of surface roughness of mild steel finished with viscoelastic magnetic abrasive medium,” *Evergreen*, 10 (*2*) 1061–1067 (2023). doi:10.5109/6793663.
11) J.K. Kim, and D.G. Lee, “Adhesion characteristics of plasma-surface-treated carbon fiber-epoxy composite with respect to release films used during demolding,” *J. Adhes. Sci. Technol.*, 18 (*4*) 473–494 (2004). doi:10.1163/156856104323016379.
12) S. H.M.S. Iqbal, Bhowmik, and R. Benedictus, “Study on the effect of surface morphology on adhesion properties of polybenzimidazole adhesive bonded composite joints,” *Int. J. Adhes. Adhes.*, 72 (*October 2016*) 43–50 (2017). doi:http://dx.doi.org/10.1016/j.ijadhadh.2016.10.002.
13) K.B. Katnam, A.J. Comer, W.F. Stanley, M. Buggy, A.R. Ellingboe, and T.M. Young, “Characterising pre-preg and non-crimp-fabric composite single lap bonded joints,” *Int. J. Adhes. Adhes.*, 31 (*7*) 679–686 (2011). doi:10.1016/j.ijadhadh.2011.06.013.

14) J. Kupski, S. Teixeira de Freitas, D. Zarouchas, P.P. Camanho, and R. Benedictus, "Composite layup effect on the failure mechanism of single lap bonded joints," *Compos. Struct.*, 217 (*December 2018*) 14–26 (2019). doi:10.1016/j.compstruct.2019.02.093.
15) D. Quan, R. Alderliesten, C. Dransfeld, I. Tsakoniatis, S. Teixeira De Freitas, G. Scarselli, N. Murphy, A. Ivanković, and R. Benedictus, "Significantly enhanced structural integrity of adhesively bonded pps and peek composite joints by rapidly uv-irradiating the substrates," *Compos. Sci. Technol.*, 199 (*July*) 108358 (2020). doi:10.1016/j.compscitech.2020.108358.
16) R. Tao, M. Alfano, and G. Lubineau, "In situ analysis of interfacial damage in adhesively bonded composite joints subjected to various surface pretreatments," *Compos. Part A Appl. Sci. Manuf.*, 116 (*June 2018*) 216–223 (2019). doi:10.1016/j.compositesa.2018.10.033.
17) M.A. Khan, G.S. Aglietti, A.D. Crocombe, A.D. Viquerat, and C.O. Hamar, "Development of design allowables for the design of composite bonded double-lap joints in aerospace applications," *Int. J. Adhes. Adhes.*, 82 (*January*) 221–232 (2018). doi:10.1016/j.ijadhadh.2018.01.011.
18) R.J. Zaldivar, H.I. Kim, G.L. Steckel, J.P. Nokes, and D.N. Patel, "The effect of abrasion surface treatment on the bonding behavior of various carbon fiber-reinforced composites," *J. Adhes. Sci. Technol.*, 26 (*10–11*) 1573–1590 (2012). doi:10.1163/156856111X618425.
19) A. Bautista, J.P. Casas-Rodriguez, M. Silva, and A. Porras, "A dynamic response analysis of adhesive - bonded single lap joints used in military aircrafts made of glass fiber composite material undercyclic impact loading," *Int. J. Adhes. Adhes.*, 102 (*April*) 102644 (2020). doi:10.1016/j.ijadhadh.2020.102644.
20) J. Zhang, X. Cheng, X. Guo, J. Bao, and W. Huang, "Effect of environment conditions on adhesive properties and material selection in composite bonded joints," *Int. J. Adhes. Adhes.*, 96 (*December 2018*) 1–7 (2020). doi:10.1016/j.ijadhadh.2018.12.001.
21) W. Huang, L. Sun, Y. Liu, Y. Chu, and J. Wang, "Effects of low-energy impact at different temperatures on residual properties of adhesively bonded single-lap joints with composites substrates," *Compos. Struct.*, 267 (*February*) 113860 (2021). doi:10.1016/j.compstruct.2021.113860.
22) M. Roy Choudhury, and K. Debnath, "Experimental analysis of tensile and compressive failure load in single-lap adhesive joint of green composites," *Int. J. Adhes. Adhes.*, 99 (*November 2019*) (2020). doi:10.1016/j.ijadhadh.2020.102557.
23) C. Hu, G. Huang, and C. Li, "Experimental and numerical study of low-velocity impact and tensile after impact for cfrp laminates single-lap joints adhesively bonded structure," *Materials (Basel).*, 14 (*4*) 1–24 (2021). doi:10.3390/ma14041016.
24) S.T. De Freitas, and J. Sinke, "Failure analysis of adhesively-bonded skin-to-stiffener joints : metal – metal vs . composite – metal," *Eng. Fail. Anal.*, 56 2–13 (2015). doi:http://dx.doi.org/10.1016/j.engfailanal.2015.05.023.
25) I.A. Akpinar, K. Gültekin, S. Akpinar, H. Akbulut, and A. Ozel, "Research on strength of nanocomposite adhesively bonded composite joints," *Compos. Part B Eng.*, 126 143–152 (2017). doi:10.1016/j.compositesb.2017.06.016.
26) C. Sun, P. Jia, C. Chen, A. Moradi, J. Zhou, M. Al Teneiji, W.J. Cantwell, and Z.W. Guan, "The effect of carbon fibre stitching on the tensile behaviour of secondary bonded single- and double-lap composite joints," *Compos. Struct.*, 265 (*December 2020*) 113774 (2021). doi:10.1016/j.compstruct.2021.113774.
27) S. Sugiman, P.D. Setyawan, S. Salman, and H. Ahmad, "Experimental and numerical investigation of the residual strength of steel-composites bonded joints: effect of media and aging condition," *Compos. Part B Eng.*, 173 (*May*) (2019). doi:10.1016/j.compositesb.2019.106977.
28) A. Fawcett, X. Chen, X. Huang, and C. Li, "Failure analysis of adhesively bonded gfrp/ aluminum matrix single composite lap joint with cold worked penetrative reinforcements," *Compos. Part B Eng.*, 161 (*July 2018*) 96–106 (2019). doi:10.1016/j.compositesb.2018.10.051.
29) K. Ramaswamy, R.M. O'Higgins, M.A. McCarthy, and C.T. McCarthy, "Influence of adhesive spew geometry and load eccentricity angle on metal-composite bonded joints tested at quasi-static and dynamic loading rates," *Compos. Struct.*, 279 (*February 2021*) 114812 (2022). doi:10.1016/j.compstruct.2021.114812.
30) S. Teixeira de Freitas, M.D. Banea, S. Budhe, and S. de Barros, "Interface adhesion assessment of composite-to-metal bonded joints under salt spray conditions using peel tests," *Compos. Struct.*, 164 68–75 (2017). doi:10.1016/j.compstruct.2016.12.058.
31) H. Grefe, M.W. Kandula, and K. Dilger, "Influence of the fibre orientation on the lap shear strength and fracture behaviour of adhesively bonded composite metal joints at high strain rates," *Int. J. Adhes. Adhes.*, 97 (2020). doi:10.1016/j.ijadhadh.2019.102486.
32) R.C. Dehaghani, D. Cronin, and J. Montesano, "Performance and failure assessment of adhesively bonded non-crimp fabric carbon fiber/epoxy composite single lap joints," *Int. J. Adhes. Adhes.*, 105 102776 (2021). doi:10.1016/j.ijadhadh.2020.102776.
33) K. Ramaswamy, R.M. O'Higgins, A.K. Kadiyala, M.A. McCarthy, and C.T. McCarthy, "Evaluation of grit-blasting as a pre-treatment for carbon-fibre

thermoplastic composite to aluminium bonded joints tested at static and dynamic loading rates," *Compos. Part B Eng.*, 185 (*January*) 107765 (2020). doi:10.1016/j.compositesb.2020.107765.

34) L. Sorrentino, W. Polini, C. Bellini, and G. Parodo, "Surface treatment of cfrp: influence on single lap joint performances," *Int. J. Adhes. Adhes.*, 85 (*May*) 225–233 (2018). doi:10.1016/j.ijadhadh.2018.06.008.
35) G. Yang, T. Yang, W. Yuan, and Y. Du, "The influence of surface treatment on the tensile properties of carbon fiber-reinforced epoxy composites-bonded joints," *Compos. Part B Eng.*, 160 (*July 2018*) 446–456 (2019). doi:10.1016/j.compositesb.2018.12.095.
36) D. Lee, Y. Oh, S. Nam, J. Choe, and D.G. Lee, "Adhesion characteristics of fiber-exposed glass composites," *Compos. Struct.*, 165 9–14 (2017). doi:10.1016/j.compstruct.2017.01.001.
37) M.R. Gude, S.G. Prolongo, and A. Ureña, "Adhesive bonding of carbon fibre/epoxy laminates: correlation between surface and mechanical properties," *Surf. Coatings Technol.*, 207 (*March 2019*) 602–607 (2012). doi:10.1016/j.surfcoat.2012.07.085.
38) K.Y. Rhee, S.G. Lee, N.S. Choi, and S.J. Park, "Treatment of cfrp by iar method and its effect on the fracture behavior of adhesive bonded cfrp/aluminum composites," *Mater. Sci. Eng. A*, 357 (*1–2*) 270–276 (2003). doi:10.1016/S0921-5093(03)00207-7.
39) M.S. Islam, L. Tong, and P.J. Falzon, "Influence of metal surface preparation on its surface profile, contact angle, surface energy and adhesion with glass fibre prepreg," *Int. J. Adhes. Adhes.*, 51 32–41 (2014). doi:10.1016/j.ijadhadh.2014.02.006.
40) A. Baldan, "Adhesion phenomena in bonded joints," *Int. J. Adhes. Adhes.*, 38 95–116 (2012). doi:10.1016/j.ijadhadh.2012.04.007.
41) X. Zhan, Y. Li, C. Gao, H. Wang, and Y. Yang, "Effect of infrared laser surface treatment on the microstructure and properties of adhesively cfrp bonded joints," *Opt. Laser Technol.*, 106 398–409 (2018). doi:10.1016/j.optlastec.2018.04.023.
42) Y. Boutar, S. Naïmi, S. Mezlini, and M.B.S. Ali, "Effect of surface treatment on the shear strength of aluminium adhesive single-lap joints for automotive applications," *Int. J. Adhes. Adhes.*, 67 38–43 (2016). doi:10.1016/j.ijadhadh.2015.12.023.
43) M. Raimondo, C. Naddeo, L. Vertuccio, K. Lafdi, A. Sorrentino, and L. Guadagno, "Carbon-based aeronautical epoxy nanocomposites: effectiveness of atomic force microscopy (afm) in investigating the dispersion of different carbonaceous nanoparticles," *Polymers (Basel).*, 11 (*5*) (2019). doi:10.3390/polym11050832.
44) L.F.M. da Silva, and R.D.S.G. Campilho, "Advances in numerical modelling of adhesive joints," Springer, 2012. doi:10.1007/978-3-642-23608-2_1.
45) F. Tahmasebi, "Automation Tools for Finite Element Bonded Joints Analysis of Adhesively Bonded Joint," in: JSME/ASME Int. Conf. Mater. Process., The Japan Society of Mechanical Engineers, Honolulu, 2002: pp. 322–326.
46) A. Bechikh, O. Klinkova, Y. Maalej, I. Tawfiq, and R. Nasri, "Effect of dry abrasion treatments on composite surface quality and bonded joints shear strength," *Int. J. Adhes. Adhes.*, 113 (*November 2021*) 103058 (2022). doi:10.1016/j.ijadhadh.2021.103058.
47) D. Gleich, "Stress Analysis of Structural Bonded Joints," Imperial College, 2002.